

## Power-dependent line shapes of transitions to autoionizing Rydberg states

S. A. Bhatti and W. E. Cooke

*Physics Department, University of Southern California, Los Angeles, California 90089-0484*

(Received 18 January 1983)

The line shapes of the  $6sns, {}^1S_0-6P_{1/2}ns$  transitions in Ba as a function of the laser intensity are modeled with the use of two-channel multichannel quantum-defect theory and the isolated-core-excitation model. An analytical expression for the line shape is derived and used to obtain a value of  $|\langle g|r|e\rangle|=4.1$  a.u. for the dipole transition moment of the  $Ba^+$  ionic  $6s-6P_{1/2}$  transition, in agreement with a recent theoretical calculation.

### INTRODUCTION

In a number of recent studies of autoionizing states of alkaline-earth atoms, the isolated-core-excitation (ICE) scheme has been used to excite the inner valence electron after the other valence electron had already been excited to a high- $n$ , Rydberg state.<sup>1,2</sup> In barium for example, a  $6snl$  Rydberg state has been excited to a  $6P_{1/2}nl$  autoionizing state by the absorption of laser light near the ionic  $Ba^+$   $6s-6P_{1/2}$  transition. Since this ionic transition has a very large oscillator strength ( $\approx 1/3$ ), it is often possible to deplete the initial  $6snl$  Rydberg state population when the laser is near the center of the  $6snl-6P_{1/2}nl$  transition, even at very low laser powers. This depletion saturates the absorption at the line center and thus gives rise to an apparent broadening of the transition.<sup>3</sup> This broadening has characteristics much like power broadening but it typically occurs at powers that are orders of magnitude smaller than that needed to power broaden a transition.

In a previous work we showed that by using this depletion broadening to increase the apparent width of an autoionizing transition, one can spectroscopically measure an autoionization rate that is smaller than the linewidth of the laser used to probe the transition.<sup>3</sup> For that analysis we used a Lorentzian line shape to represent the natural, unbroadened transition. However, for autoionizing Rydberg states there are additional complications due to satellite transitions, such as  $6snl-6P_{1/2}(n\pm 1)l$ . These satellites not only give extra peaks, but also affect the signal size between peaks and produce asymmetries since a proper sum over all transition moments must be done.

In this work, we will show that the  $6s20s {}^1S_0-6P_{1/2}ns$  transition can be well modeled over a power range of two orders of magnitude above that required to depletion broaden the line, by using a two-channel multichannel quantum-defect theory<sup>4</sup> (MQDT) to sum the satellites properly and an ICE transition moment model.<sup>5</sup>

In the following section an analytical expression for the depletion broadening of a transition is derived using ICE and MQDT. The experimental technique and data showing the line shapes of the  $6s20s {}^1S_0-6P_{1/2}ns, J=1$  transition in barium as a function of laser intensity are presented in the third section. In the final section the data and theory are compared and a value for the transition moment for the  $6s-6P_{1/2}$  transition in the barium ion is deduced.

### THEORY

The wave function of a two electron atom in a bound Rydberg state consists predominantly of a single configuration having an unexcited core electron and a highly excited Rydberg electron. Owing to the large value of the principal quantum number  $n$ , the Rydberg electron spends most of its time orbiting far away from the core. The core electron, therefore, responds strongly to optical frequencies close to the resonant frequencies of the  $Ba^+$  ion. When a bound Rydberg state absorbs an additional optical photon to excite its core electron, the atom is promoted to an autoionizing state.

The cross section for such a process is comparable ( $\approx 10^{-17}$  cm<sup>2</sup>) to that for a bound-bound transition and is therefore usually much larger than the cross section for direct photoionization of the Rydberg electron (which is very close to the ionization threshold). However, when the core electron makes a transition, the Rydberg electron suddenly sees a potential due to a different core structure and finds itself in a superposition state formed from the new Rydberg series whose quantum defect matches the new boundary conditions at the new core. Using the isolated-core-excitation model, which merely projects the initial Rydberg wave function onto the new Rydberg series,<sup>5</sup> it has been shown that the dipole transition moment for such a transition is given by

$$\mu = \langle gn_g^*l | r | en_e^*l' \rangle = \langle g | r | e \rangle \langle n_g^*l | n_e^*l' \rangle \quad (1a)$$

$$= \frac{1}{3} \langle g | r | e \rangle \delta_{ll'} (n_g^* n_e^*)^{-3/2} \frac{\sin[\pi(n_e^* - n_g^*)]}{\pi(W_e - W_g)}, \quad (1b)$$

$$W = \frac{-1}{2n^{*2}}. \quad (1c)$$

Here  $\langle g | r | e \rangle$  is the transition moment for the isolated ion transition from the ground state  $g$  to excited state  $e$ . The Rydberg electron's initial and final state is represented by  $n_g^*l$  and  $n_e^*l'$ , respectively, where  $n_g^*$  and  $n_e^*$  are effective quantum numbers and  $W_g$  and  $W_e$  are the energies of these states relative to ionization limits which correspond to the ground and excited states of the ion.  $\delta_{ll'}$  is the Kronecker  $\delta$  function. The factor  $\frac{1}{3}$  appearing in

front of equation (1b) is a geometric factor for the transitions we are interested in, namely,  $6s20s^1S_0-6P_{1/2}ns$ ,  $J=1$ . It depends entirely upon the angular momenta coupling and the laser polarization, and in general will be different from case to case.

In the autoionizing region of the spectrum, a wave function cannot be properly represented by a single configuration since at least some admixture of a continuum configuration is required to account for the autoionization process. A two-channel MQDT wave function which allows for this continuum admixture can be written as<sup>4</sup>

$$\psi = (n_e^*)^{3/2} A_e \chi_e \phi(n_e^* l) + \chi_g \phi(\epsilon l), \quad (2)$$

where  $\chi$  represents the core wave function (either excited or ground) and  $\phi$  is a Coulomb wave function. In the first term, the Coulomb wave function is bound and has an effective quantum number  $n_e^*$  while in the second term, the Coulomb wave function is unbound, having energy  $\epsilon$ .  $A_e$  is the relative admixture of the bound channel. The  $(n_e^*)^{3/2}$  factor normalizes the bound wave function per unit energy, as is appropriate for a continuum wave function. The expression for the dipole moment, therefore, has to be modified by  $(n_e^*)^{3/2} A_e$ . The square of the dipole moment will also be normalized per unit energy. Note that the decaying of an autoionizing state to an electron-ion pair is automatically taken into account by the MQDT mixed wave function. For two channels, the MQDT expression for  $A_e$  is

$$A_e = -R \left[ \frac{1 + \epsilon_e^2}{\epsilon_e^2 + R^4} \right]^{1/2}, \quad (3a)$$

$$\epsilon_e = \tan[\pi(n_e^* + \delta_e)]. \quad (3b)$$

Here  $R$  represents the interaction between the continuum and bound configurations and  $\delta_e$  is the quantum defect of the doubly excited, autoionizing Rydberg series.

Because the tangent function is cyclic,  $A_e$  has a series of peaks separated by integer changes in the value of  $n_e^*$ . Each peak is approximately Lorentzian for values of  $n_e^* + \delta_e$  near an integer. For small  $R$ , the spectral full width at half maximum (FWHM) for each peak may be identified:

$$\Gamma = \frac{2R^2}{\pi(n_e^*)^3}. \quad (4)$$

The  $(n_e^*)^{-3}$  factor accounts for decreasing energy spacing between peaks as  $n_e$  increases. This FWHM is normally attributed to lifetime broadening of the doubly excited state due to the rapid autoionization process.

The number of electron-ion pairs produced by a laser pulse of duration  $\tau$  and electric field  $\mathcal{E} \exp(-i\omega t)$  then would be

$$N = N_0 [1 - \exp(-2\pi |\Omega|^2 \tau)], \quad (5a)$$

$$|\Omega|^2 = |\mu \mathcal{E}|^2, \quad (5b)$$

where the modified expression for the square of the dipole moment is

$$\mu^2 = \frac{1}{9} |\langle g | r | e \rangle|^2 \frac{\sin^2[\pi(n_e^* - n_g^*)]}{\pi^2(n_e^*)^3 (W_e - W_g)^2} R^2 \frac{1 + \epsilon_e^2}{\epsilon_e^2 + R^4} \quad (6)$$

and we used Fermi's golden rule to evaluate the transition rate.<sup>6</sup> Again, note that  $|\mu \mathcal{E}|^2$  has units of inverse time, due to the continuum normalization of the wave function. The first factor has the largest contribution when the argument  $\pi(n_e^* - n_g^*)$  of the sine function is near zero. The other maxima decrease in size rapidly because of the energy denominator. The second factor is the MQDT lineshape factor representing the series of Rydberg state resonances. For large powers the central peak (where  $n_e^* \approx n_g^*$ ) saturates as the exponential function in Eq. (5a) approaches zero, representing the depletion of the initial state. However, the side peaks, where

$$n_e^* + \delta_e \approx n_g^* + \delta_g \pm 1,$$

will then show up. For small powers where the main maxima cannot make the exponential function vanish, the side peaks will usually be very small. Therefore, for small powers the most interesting part of the spectrum is where  $n_e^* + \delta_e$  is close to an integer. For such a situation the sine, tangent, and exponential functions can be replaced by their arguments so that

$$N \approx N_0 \frac{|\langle g | r | e \rangle|^2 \tau}{9\pi} \frac{\Gamma/2}{(W_e - W_g)^2 + (\Gamma/2)^2} \quad (7)$$

which is the Lorentzian referred to earlier. At lower power densities, therefore, the use of only one broadened transition is justified.

## EXPERIMENT

We studied the  $6s20s^1S_0-6P_{1/2}ns$ ,  $J=1$  absorption by measuring the ionization of an effusive atomic beam of excited  $6s20s^1S_0$  barium atoms. The atomic beam passes between two parallel plates (Fig. 1), where two lasers, one at the  $6s^2^1S_0-6s6p^1P_1$  (5536 Å) resonant transition and one at the  $6s6p^1P_1-6s20s^1S_0$  (4248 Å) transition, excite the atoms to the Rydberg states as shown in Fig. 2. A third tunable laser near the  $Ba^+ 6s-6P_{1/2}$  transition, then drives the  $6s20s^1S_0-6P_{1/2}ns$ ,  $J=1$  transition to produce autoionizing states. We measured the total absorption of the third laser by collecting the electrons produced by the autoionizing atoms, since all but a very small fraction ( $10^{-5}$ ) of the atoms produce ion-electron pairs rather than reradiate to bound states. A small voltage (5 V) on the bottom plate drives the electrons through a hole in the top plate, through a small collimating magnetic field, and to a channeltron detector. By reversing the collection voltage, we could alternatively collect ions (which are essentially unaffected by the magnetic field) and obtain similar results.

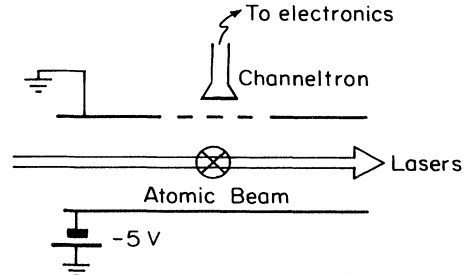


FIG. 1. Schematic diagram of the experiment.

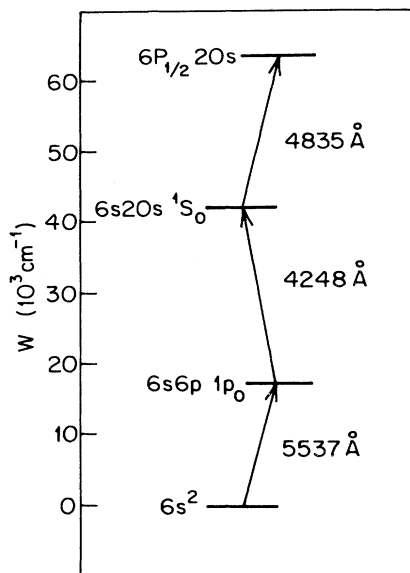


FIG. 2. Excitation diagram. The arrows represent the three laser excitations. The first ionization limit for Ba is at  $42032.4 \text{ cm}^{-1}$ .

Each of the three laser pulses arrived slightly delayed from the previous one in order to avoid any possible spectrum complications due to *ac* Stark effects.<sup>7</sup> All three lasers had the same linear polarization, 5 ns duration and a linewidth of  $0.4 \text{ cm}^{-1}$  or better. The  $5536 \text{ Å}$  laser had a very weak focus of  $1.0 \text{ cm}^2$  since so little power was needed to saturate the first transition. The second laser had a focus of  $\frac{1}{2} \text{ mm}^2$  to accurately define the interaction region, while the third laser had again a weak focus of  $0.9 \text{ cm}^2$ . This ensured that the third laser power density was uniform over the entire interaction region. We directly measured the absolute power density of the third laser by passing it through a calibrated aperture and measuring the output with a Scientech model-380101 energy meter. The typical maximum power density was  $29 \text{ kW/cm}^2$ , although this value varied by 20% approximately linearly over the tuning range used for the third laser scan. We used calibrated neutral density filters to vary the third laser's relative power.

A computer controlled stepping-motor scanned the third laser while part of the beam was split off and passed through a  $1.68 \text{ cm}^{-1}$  free-spectral range (FSR) etalon to calibrate its relative wavelength. At  $20207.49 \text{ cm}^{-1}$  a two-photon resonance

$$6s6p\ ^1P_1 - 6s9d\ ^1D_2 - 6P_{1/2}9d$$

served as an absolute wavelength calibrator.<sup>2</sup> The spectrum, and the etalon marker, were converted using 12-bit (binary digit) analog-to-digital converters (A/D's) and stored on a floppy disk. To account for the nonlinearities in the laser scan rate, a computer program interpolated the data to obtain a constant number of data points between successive etalon peaks.

To compare Eq. (5a) to the data, we obtained a value for  $N_0$  from the maximum of the highest-power scan. Since the wavelength (or energy) scale was calibrated absolutely

by the interpolated data and the two-photon marker resonance, the only remaining parameters in Eq. (5a) are those relating to the atomic structure. Three of these are documented already in the literature, namely, the effective quantum number of the  $6P_{1/2}20s, J=1$  state,<sup>8</sup>  $n_0^* = 15.696$  (or  $\delta_e = 4.304$ ), the effective quantum number of  $6s20s\ ^1S_0$  state,  $n_g^* = 15.809$  (or  $\delta_g = 4.191$ ), and the natural linewidth of the  $6P_{1/2}20s, J=1$  state,  $\Gamma = 3.1 \text{ cm}^{-1}$  (or  $R^2 = 0.0857$ ).<sup>3</sup> We chose the last parameter, the square of the dipole moment of the ionic transition  $\text{Ba}^+ 6s - \text{Ba}^+ 6P_{1/2}$ ,  $|\langle g | r | e \rangle|^2$ , to fit the width of the highest-power data scan, leaving no adjustable parameter for the successive low-power scans. In using Eq. (5) we accounted for the observed 20% decrease in our laser's output power at the lower-wavelength end of the spectrum, by using a linear power decrease with frequency.

## DISCUSSION

Figure 3 shows the comparison of Eq. (5a) and data using a value of  $|\langle g | r | e \rangle| = 4.1 \text{ a.u.}$  Over two orders of magnitude, even though the shape of the spectrum changes dramatically, the data and our model are in excellent agreement. In particular, notice the detailed agreement in the shapes, asymmetries, widths, and heights of the different peaks. The narrow peak at  $n^* \approx 14.9$  is the two-photon calibration transition referred to above. The major source of uncertainty in this measurement is the power density which we estimate is accurate to better than 15%. Since our fits are insensitive to a 5% variation in the value of the  $|\langle g | r | e \rangle|^2$ , we estimate a 15% uncer-

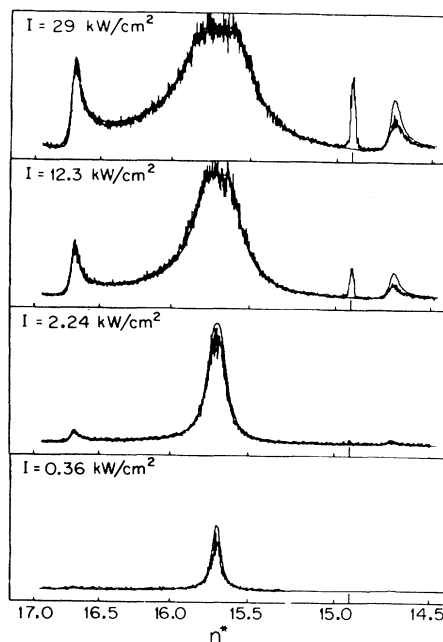


FIG. 3. Experimental data and comparison to theory for various laser powers. The vertical axis is the total number of detected electrons and has the same normalization for each plot. The horizontal scale is the effective quantum number  $n^*$  relative to the  $\text{Ba}^+ 6P_{1/2}$  ionization limit. A change of 0.1 in  $n^*$  represents about a  $1.3 \text{ Å}$  change in laser wavelength. The feature at  $n^* \approx 14.9$  is the two-photon resonance at  $20207.49 \text{ cm}^{-1}$  which was used as the absolute wavelength reference.

tainty in our value of the  $|\langle g | r | e \rangle|^2$ . A value of  $|\langle g | r | e \rangle| = 4.3$  has been calculated using Coulomb wave functions, and empirical  $\text{Ba}^+$  energy level data.<sup>9</sup>

The height of the peak on the long wavelength side of the spectrum, which is due to a transition to the  $6P_{1/2}19s$ ,  $J=1$  state, is smaller than our model predicts. The reason for this discrepancy becomes clear when we look at Eq. (6) again. The asymmetries and heights of the side peaks are extremely sensitive to how close they are to the zeros of the sine function. Our model, which is based upon a two-channel MQDT, assumes the same quantum defect for the whole Rydberg autoionizing series. The experimental value for the quantum defect for the  $6P_{1/2}19s$ ,  $J=1$  is, however, slightly greater (by 0.02).<sup>10</sup> This slight increase in the quantum defect of  $6P_{1/2}19s$ ,  $J=1$  pulls it slightly towards the zero of the sine function resulting in an appropriate reduction of the height of the  $6P_{1/2}19s$ ,  $J=1$

peak. We did not incorporate this into our model, since that would require more than two channels and the discrepancy is not sufficiently severe to determine the additional atomic parameters that would be required. However, this extreme sensitivity suggests that it might be more accurate to measure the quantum defects of autoionizing states, by measuring their amplitude in a satellite transition. Such a technique has been used recently by Tran *et al.*<sup>11</sup>

#### ACKNOWLEDGMENTS

This work was supported by the National Science Foundation, under Grant No. PHY-82-01688. Some of the equipment was provided by the Research Corporation. One of us (W.E.C) wishes to acknowledge support through an Alfred P. Sloan Foundation Fellowship.

<sup>1</sup>W. E. Cooke, T. F. Gallagher, S. A. Edelstein, and R. M. Hill, Phys. Rev. Lett. **40**, 178 (1978).

<sup>2</sup>W. E. Cooke and T. F. Gallagher, Phys. Rev. Lett. **41**, 1648 (1978).

<sup>3</sup>W. E. Cooke, S. A. Bhatti, and C. L. Cromer, Opt. Lett. **7**, 69 (1982).

<sup>4</sup>M. J. Seaton, Rep. Prog. Phys. **46**, 167 (1983); U. Fano, Phys. Rev. A **2**, 353 (1970). Fano's formalism uses parameters  $\mu_1$ ,  $\mu_2$ , and  $\theta$  (where  $\theta$  is the rotation angle for a  $2 \times 2$  unitary matrix). They are related to our parameters  $R$ ,  $\delta_e$ , and  $\delta_c$  in the following way:

$$\tan(2\theta) = \frac{2R}{(1-R^2)} \csc[\pi(\delta_c - \delta_e)],$$

$$\tan(\pi\mu_2) + \tan(\pi\mu_1) = \frac{(1+R^2)\sin[\pi(\delta_c + \delta_e)]}{\cos(\pi\delta_e)\cos(\pi\delta_c) - R^2\sin(\pi\delta_e)\sin(\pi\delta_c)},$$

$$\begin{aligned} \tan(\pi\mu_2) - \tan(\pi\mu_1) \\ = \frac{(1-R^2)\sin[\pi(\delta_c - \delta_e)]}{\cos(2\theta)[\cos(\pi\delta_e)\cos(\pi\delta_c) - R^2\sin(\pi\delta_e)\sin(\pi\delta_c)]}. \end{aligned}$$

Here  $\delta_c$  is the phase shift of an unperturbed continuum relative to a hydrogenic continuum. Note that this parameter does not appear in our equations for the spectrum and therefore, cannot be measured using this technique.

<sup>5</sup>S. A. Bhatti, C. L. Cromer, and W. E. Cooke, Phys. Rev. A **24**, 161 (1981).

<sup>6</sup>L. I. Schiff, *Quantum Mechanics*, 3rd ed. (McGraw-Hill, New York, 1968).

<sup>7</sup>T. A. Georges and P. Lambropoulos, Phys. Rev. A **15**, 727 (1977).

<sup>8</sup>J. R. Rubbmark, S. A. Borgstrom, and K. Bockasten, J. Phys. B **10**, 421 (1977).

<sup>9</sup>A. Lindgard and S. E. Nielsen, At. Data Nucl. Data Tables **19**, 533 (1977).

<sup>10</sup>C. L. Cromer, S. A. Bhatti, and W. E. Cooke, Bull. Am. Phys. Soc. **25**, 1134 (1980).

<sup>11</sup>N. H. Tran, R. Kachru, and T. F. Gallagher, Phys. Rev. A **26**, 3016 (1982).